

Distinct mechanisms for diastolic dysfunction in diabetes mellitus and chronic pressure-overload

Inês Falcão-Pires · Giuseppina Palladini · Nádia Gonçalves · Jolanda van der Velden · Daniel Moreira-Gonçalves · Daniela Miranda-Silva · Francesco Salinaro · Walter J. Paulus · Hans W. M. Niessen · Stefano Perlini · Adelino F. Leite-Moreira

Received: 23 August 2010/Revised: 7 March 2011/Accepted: 20 April 2011/Published online: 1 May 2011
© Springer-Verlag 2011

Abstract Chronic pressure-overload and diabetes mellitus are two frequent disorders affecting the heart. We aimed to characterize myocardial structural and functional changes induced by both conditions. Pressure-overload was established in Wistar-han male rats by supra-renal aortic banding. Six-weeks later, diabetes was induced by streptozotocin (65 mg/kg,ip), resulting in four groups: SHAM, banding (BA), diabetic (DM) and diabetic-banding (DB). Six-weeks later, pressure–volume loops were obtained and left ventricular samples were collected to evaluate alterations in insulin signalling pathways, extracellular matrix as well as myofilament function and phosphorylation. Pressure-overload increased cardiomyocyte diameter (BA $22.0 \pm 0.4 \mu\text{m}$, SHAM $18.2 \pm 0.3 \mu\text{m}$) and myofilament maximal force (BA $25.7 \pm 3.6 \text{ kN/m}^2$, SHAM $18.6 \pm 1.4 \text{ kN/m}^2$), Ca^{2+} sensitivity (BA 5.56 ± 0.02 , SHAM

5.50 ± 0.02) as well as MyBP-C, Akt and Erk phosphorylation, while decreasing rate of force redevelopment (K_{tr} ; BA $14.9 \pm 1.1 \text{ s}^{-1}$, SHAM $25.2 \pm 1.5 \text{ s}^{-1}$). At the extracellular matrix level, fibrosis (BA $10.8 \pm 0.9\%$, SHAM $5.3 \pm 0.6\%$), pro-MMP-2 and MMP-9 activities increased and, in vivo, relaxation was impaired (τ ; BA $14.0 \pm 0.9 \text{ ms}$, SHAM $12.9 \pm 0.4 \text{ ms}$). Diabetes increased cardiomyocyte diameter, fibrosis (DM $21.4 \pm 0.4 \mu\text{m}$, $13.9 \pm 1.8\%$, DB $20.6 \pm 0.4 \mu\text{m}$, $13.8 \pm 0.8\%$, respectively), myofilament Ca^{2+} sensitivity (DM 5.57 ± 0.02 , DB 5.57 ± 0.01), advanced glycation end-product deposition (DM $4.9 \pm 0.6 \text{ score/mm}^2$, DB $5.1 \pm 0.4 \text{ score/mm}^2$, SHAM $2.1 \pm 0.3 \text{ score/mm}^2$), and apoptosis, while decreasing K_{tr} (DM $13.5 \pm 1.9 \text{ s}^{-1}$, DB $15.2 \pm 1.4 \text{ s}^{-1}$), Akt phosphorylation and MMP-9/TIMP-1 and MMP-1/TIMP-1 ratios. Diabetic hearts were stiffer (higher end-diastolic-pressure: DM $7.0 \pm 1.2 \text{ mmHg}$, DB $6.7 \pm 0.7 \text{ mmHg}$, SHAM $5.3 \pm 0.4 \text{ mmHg}$, steeper end-diastolic-pressure–volume relation: DM 0.59 ± 0.18 , DB 0.83 ± 0.17 , SHAM 0.41 ± 0.10), and hypo-contractile (decreased end-systolic-pressure-volume-relation). DB animals presented further pulmonary congestion (Lungs/body-weight: DB $5.23 \pm 0.21 \text{ g/kg}$, SHAM $3.80 \pm 0.14 \text{ g/kg}$) as this group combined overload-induced relaxation abnormalities and diabetes-induced stiffness. Diabetes mellitus and pressure overload led to distinct diastolic dysfunction phenotypes: while diabetes promoted myocardial stiffening, pressure overload impaired relaxation. The association of these damages accelerates the progression of diastolic heart failure progression in diabetic-banded animals.

I. Falcão-Pires · N. Gonçalves · D. Moreira-Gonçalves · D. Miranda-Silva · A. F. Leite-Moreira (✉)
Department of Physiology and Cardiothoracic Surgery, Cardiovascular R&D Unit, Faculty of Medicine, University of Porto, Alameda Professor Hernâni Monteiro, 4200-319 Porto, Portugal
e-mail: amoreira@med.up.pt

G. Palladini · F. Salinaro · S. Perlini
Clinica Medica II, Fondazione IRCCS San Matteo, Università di Pavia, Pavia, Italy

J. van der Velden · W. J. Paulus
Department of Physiology, Institute for Cardiovascular Research, Vrije University Medical Center Amsterdam, Amsterdam, The Netherlands

H. W. M. Niessen
Pathology and Surgery, Vrije University Medical Center, Amsterdam, The Netherlands

Keywords Diabetes mellitus · Diastolic function · Hypertrophy · Myocardial stiffness · Pressure-overload · Relaxation

Introduction

Diastolic left ventricular (LV) dysfunction importantly contributes to heart failure (HF) with normal ejection fraction (EF) [17]. Diastolic dysfunction is usually ascribed to impaired relaxation or abnormal myocardial passive properties [23, 52]. This condition, which has a poor prognosis, represents nearly half of the hospitalizations for HF and a growing problem in industrialized nations [52].

Experimental and clinical evidences show that diabetes mellitus is associated with abnormalities of systolic and diastolic performance [52]. The streptozotocin (STZ)-induced diabetic rat, a hypoinsulinemic model of type 1 diabetes, has been used to define the pathophysiology of hyperglycaemic conditions [25, 41], showing significant changes in cardiomyocytes and myocardial mechanical properties such as prolongation of contraction and relaxation [5, 32]. Functionally, this altered kinetic has been mostly attributed to impaired intracellular Ca^{2+} homeostasis [9]. Additionally, changes in the intrinsic passive properties of the heart, such as advanced glycation end-products (AGE) [3] and collagen [44] deposition induce extracellular matrix (ECM) abnormalities hence, contributing to increased stiffness and impaired ventricular filling [52]. Furthermore, matrix metalloproteinases (MMP) and their tissue-specific inhibitors (TIMP) regulate a complex balance between collagen degradation and its deposition, therefore contributing to matrix remodelling in several cardiac diseases [28] such as in diabetic cardiomyopathy. AGE receptors, RAGE, are currently being object of many investigations due to their role in promoting inflammation and fibrosis in hyperglycaemic conditions. Moreover, many of the current antifibrotic therapies exert their effects via RAGE modulation [20, 46].

Another frequent cause for HF is chronic pressure-overload. Over 10% of the population suffers from severe hypertension. Initially, it induces myocardial hypertrophy as an adaptative response by which the LV compensates for increased afterload [13]. Longstanding pressure-overload, however, results in myocardial systolic and diastolic dysfunction, structural damages and, later on, congestive HF [1, 7]. Despite improvements in anti-hypertensive treatment, therapy-resistant hypertension often leads to cardiac failure.

Hypertension is more prevalent among the diabetic population and exacerbates the extent of diabetic cardiomyopathy [10, 25, 41]. Even so, functional and structural cardiac consequences of combined hypertension and diabetes are still unclear, especially those related with changes in single cardiomyocytes, in the ECM, size of the ventricular chamber and diastolic function. So far, the results are conflicting reporting either increased [31] or decreased myocardial stiffness [33].

Additionally, it is currently accepted that insulin exerts its pro-hypertrophic effects on responsive tissues such as the myocardium both in diabetic and in overloaded hearts. These effects mediate hypertrophy by distinct mechanisms: insulin activates Akt-1 pathway that mediates glucose uptake. Akt-1 phosphorylates and inactivates glycogen synthases kinase-3 β (GSK-3 β), a well-recognized inhibitor of nuclear transcription governing the hypertrophic process via the nuclear factor of activated T-cells (NFAT) [30]. In addition, there are other insulin-mediated, but Akt-1-independent, pathways that may be operative, most notably the extracellular signal-regulated kinase (ERK)/mitogen-activated protein (MAP) kinase pathways [30]. Significant cellular evidence exists for an insulin-induced activation of the p38 MAP kinase pathway. Therefore, we explored insulin signaling pathways underlying the functional changes induced by diabetes and chronic pressure overload.

The present study aimed to analyse and describe the myocardial morphological and functional changes induced by diabetes and/or pressure-overload from an integrative perspective that is studying changes at the molecular, cellular and intact heart level, particularly in terms of insulin signalling pathways, force measurements in isolated cardiomyocytes, phosphorylation status of myoflamentary proteins, ECM and in vivo pressure–volume haemodynamics.

Materials and methods

Animal models

All animal experiments were performed according to the Portuguese law for animal welfare and accordingly to the Guide for the Care and Use of Laboratory Animals published by the National Institutes of Health (NIH Publication 85-23, Revised 1996). The Faculty of Medicine of Porto is a governmental institution, granted approval by the Portuguese government to perform animal experiments. Male Wistar-han rats were housed in groups of 4 animals per cage in a controlled environment under a 12:12-h light–dark cycle at a room temperature of 22°C, with free supply of food and water.

After an overnight fast, rats were anaesthetized with an intraperitoneal injection of ketamine:xylazine (75:5 mg/kg) and surgical banding was performed as previously described [28]. Six weeks after surgery, rats fasted for 5 h were randomly injected with STZ (65 mg/kg, ip) or an equal volume of citrate buffer (pH = 4.5). One week later, diabetic state was assessed by measurement of non-fasting serum glucose concentration. This resulted in four experimental groups: SHAM ($n = 10$), banded (BA, $n = 10$),

diabetic (DM, $n = 14$) and diabetic-banded (DB, $n = 14$). We started by inducing pressure overload as this model provides a gradual injury that takes several weeks to develop considerable myocardial hypertrophy and, therefore, progressing slower than the fast STZ-diabetic model. This way, we chose to induce first chronic pressure overload and latter, diabetes mellitus. Twelve weeks after the surgical procedure, haemodynamic evaluation with conductance catheters was performed.

Haemodynamic measurements

Instrumentation

Rats were anaesthetized by inhalation with a mixture of 4% sevoflurane with oxygen, intubated for mechanical ventilation (respiratory frequency 100 min^{-1} and weight-adjusted tidal volume; Harvard Small Animal Ventilator-Model 683) and placed over a heating pad (37°C). The right jugular vein was cannulated for fluid administration (prewarmed 0.9% NaCl solution) to compensate for perioperative fluid losses. A median sternotomy was performed to expose the heart and the pericardium was widely opened. A 2F microtip pressure–volume conductance catheter (SPR-838, Millar Instruments) was inserted by an apical puncture into the LV cavity along its long axis. The catheter was connected to MVP-300 conductance system (Millar Instruments), coupled to PowerLab16/30 converter (AD Instruments) and a personal computer for data acquisitions. After complete instrumentation, the animal preparation was allowed to stabilize for 15 min. Haemodynamic recordings were made with respiration suspended at the end of expiration under steady-state conditions or during preload reductions (vena cava occlusion). Parameters from conductance catheter were recorded at a sampling rate of 1,000 Hz, in order to accurately capture all of the features of the pressure–volume waveforms produced by the fast-beating rat hearts. Data were stored and analyzed with Millar conductance data acquisition and analysis software (PVAN3.5).

Measured parameters

Heart rate, stroke volume, end-diastolic volume ($LV-V_{ED}$), end-systolic volume ($LV-V_{ES}$), EF, end-diastolic pressure ($LV-P_{ED}$) and end-systolic pressure ($LV-P_{ES}$) were determined from the pressure–volume tracings. Effective systemic arterial elastance (E_a), as a measure of LV afterload, was calculated dividing $LV-P_{ES}$ by stroke volume. Maximal LV wall-stress [$LV-W_{STRESS}$] was calculated from LV pressure [$P(t)$] and volume [$V(t)$] and LV wall volume (V_{wall}) according to the following formula: $LV-W_{STRESS} = P(t)\{1 + 3[V(t)/V_{wall}]\}$ [16]. LV wall volume

(V_{wall}) was approximated as the sum of the LV free wall mass and half of the interventricular septum mass. Relaxation rate was estimated with the time constant τ using the Glantz method.

The intrinsic myocardial function relatively load-independent parameters LV end-systolic pressure–volume relation (ESPVR) and end-diastolic pressure–volume relation (EDPVR) were determined from pressure–volume loops recorded during transient occlusion of the inferior vena cava by external compression of the vessel.

Conductance calibration

Parallel conductance values were obtained by the injection of approximately 100 μl of 10% NaCl into the right atrium. Calibration from relative volume units (RVU) conductance signal to absolute volumes (μl) was undertaken using a previously validated method of comparison to known volumes in Perspex wells [50].

Morphometric analysis and tissue preparation

After haemodynamic data collection, the anaesthetized animals were sacrificed through cardiectomy and exsanguination. The heart, lung and LV + septum (LV + S) were dissected, weighed separately, normalized to body weight (BW) and divided in two fragments: one was immediately frozen with liquid nitrogen to preserve the phosphorylation status, and the other stored in 10% formalin for histological analysis.

Quantitative histomorphometry and extracellular matrix analysis

Histomorphological analysis of LV samples was performed on Picrosirius red and haematoxylin-and-eosin-stained 4- μm -thick-sections of tissue placed in 10% formalin. Section images were acquired with a microscope ($\times 50$) and analysed with Slidebook 4.0 software (3I, Denver, Colorado) to determine cardiomyocyte diameter and myocardial fibrosis. As previously described and validated [43], cardiomyocyte diameter was calculated by averaging over 15 representative cardiomyocytes per animal (SHAM $n = 5$, DM $n = 4$, BA $n = 5$ and DB $n = 5$) after measuring the diameter perpendicularly to the outer contour of the cell at the nucleus level. Picrosirius-red staining is widely used to evaluate myocardial fibrosis. Red staining with Picrosirius is accompanied by a pronounced increase in birefringence, which is an unequivocal indication of the presence of collagen and reticulin fibres [21, 48]. We dewaxed and hydrated paraffin sections, stained 4- μm -slide with picro-Sirius red for 1 h, followed by two washes with acidified water. Finally, we dehydrated in 80, 90 and three

changes of 100% ethanol, cleared in xylene and mounted in a resinous medium. We examined the sections on a polarized microscope ($\times 400$) always using similar light intensity and photographed the slides using a digital camera. Slidebook software was used to calculate the sum of all connective tissue areas divided by the sum of connective tissue and muscle areas averaged over 4–6 representative fields of the section. Areas of reparative and perivascular fibrosis were excluded. The intensity of the red colour can be measured by microdensitometry to provide estimates of collagen content in different parts of a tissue.

Quantification of the AGE *N*- ϵ (carboxymethyl)lysine (CML) was performed using a specific anti-CML monoclonal antibody as previously described [37].

LV myocardial MMP extraction, zymography and immunoblotting as well as TIMPs quantification was performed on 6 SHAM, 6 BA, 6 DM and 6 DB rats [28]. Briefly, to detect MMP lytic activity, the myocardial extracts were loaded onto electrophoretic gels (SDS-PAGE) containing 1 mg/mL of gelatin or collagen (type III denatured), under nonreducing conditions. Gels were run at 15 mA/gel through the stacking phase (4%) and at 20 mA/gel for the separating phase (10%), at 4°C in a running buffer. The gels were stained with Coomassie blue R-250 for 30 min and destained by changing the solution for 60 min, to be subsequently dried and analyzed, looking for zones of enzymatic activity as indicated by negative staining. In all zymograms, prestained molecular weight markers (Novex, San Diego, CA) and positive controls (Oncogene, San Diego, CA) were included. The zymograms were analysed by a densitometer (GS710 Densitometer; Bio-Rad, Hercules, CA) and data were expressed as optical density (OD), reported to 1 mg/mL protein content.

The TIMP-1 and TIMP-2 assays were performed by commercial ELISA kits (Biotrak; Amersham Pharmacia Biotech-England) that detect total TIMP-1 or TIMP-2. TIMP concentrations were expressed as ng/ml reported to mg/ml of proteins of each sample.

Force measurements in isolated cardiomyocytes

Force measurements were performed in single, triton-permeabilized cardiomyocytes mechanically isolated from LV free wall samples as described previously [4, 43], in which active (F_{active}) and passive forces (F_{passive}) were measured to detect systolic and/or diastolic dysfunction at the myofilament level.

In brief, biopsy samples were defrosted in relaxing solution (free of Ca^{2+}), mechanically disrupted and incubated for 5 min in relaxing solution supplemented with 0.2% Triton X-100 to remove all membrane structures. Subsequently, cardiomyocytes were washed and attached between a force transducer and a motor (~ 3

cardiomyocytes per animal for a total of 5 SHAM, 5 BA, 5 DM and 5 DB LV samples). After setting sarcomere length (SL) at 2.2 μm , the myocytes were subjected to both relaxing and Ca^{2+} activating solutions. Their pCa ($-\log_{10}[\text{Ca}^{2+}]$) ranged from 9.0 (relaxing) to 4.5 (maximal activation) to produce a force-pCa relation. Maximal activation at pCa 4.5 was used to calculate maximal calcium-activated isometric force. After transferring the cardiomyocyte from relaxing to activating solution, isometric force started to develop (F_{total}). Once a steady-state force level was reached, the cell was shortened within 1 ms to 80% of its original length (slack test) to determine the baseline of the force transducer. The distance between the baseline and the steady force level is F_{total} . After 20 ms, the cell was re-stretched and returned to the relaxing solution, in which a second slack test of 10-s duration was performed to determine resting or F_{passive} . The slack test at pCa = 4.5 allowed to measure the rate of force-redevelopment (K_{tr}) since this manoeuvre resulted in the complete dissociation of cross-bridges from actin, so that the subsequent redevelopment of tension was related to the rate of cross-bridge reattachment.

mRNA quantification

For gene expression analyses, RNA was extracted with TriPure (Roche). RT-PCR was performed with total RNA, followed by real-time PCR analyses using the SYBR Green method in a LightCycler 2.0 (Roche).

For the animal studies, results are relative to the mean obtained for the SHAM group (set as arbitrary unit) and normalized for glyceraldehyde-3-phosphate dehydrogenase (GAPDH). Specific PCR primer pairs for the studied genes were GAPDH, sarcoplasmic reticulum Ca^{2+} -ATPases-2a (SERCA2a), phospholamban (PLB), tumor necrosis-factor- α (TNF- α), transforming growth factor- β_1 (TGF- β_1), myosin heavy-chain- α (MHC- α) and myosin heavy-chain- β (MHC- β).

Myofilament protein phosphorylation

Myofilament protein phosphorylation was determined in myocardial samples from five samples of each group using Pro-Q Diamond Phosphoprotein Stain. To preserve the endogenous phosphorylation status, frozen biopsies were homogenized in 1 ml cold 10% trichloroacetic acid solution [TCA, dissolved in acetone containing 0.1% (w/v) dithiothreitol (DTT)]. TCA-treated tissue pellets were homogenized in sample buffer containing 15% glycerol, 62.5 mmol/l Tris (pH 6.8), 1% (w/v) SDS and 2% (w/v) DTT (final concentration 2.5 μg dry weight/ μl). Tissue samples (25 μg dry weight/lane) were separated on gradient gels (Criterion, tris-HCl 4–15% gel, BioRad) and

proteins stained for 1 hour with Pro-Q Diamond Phospho-protein Stain. Fixation, washing and de-staining were performed according to manufacture's guidelines (Molecular Probes) [51]. Phosphorylation status of myofilament proteins was expressed relative to each SYPRO-stained protein content to correct for differences in sample loading and expressed in arbitrary units (AU). Staining was visualized using the LAS-3000 Image reader (Fuji, 460 nm/605 nm Ex/Em) and signals were analysed with AIDA software.

Western blot analysis

LV samples from of each group (SHAM $n = 4$, DM $n = 5$, BA $n = 4$ and DB $n = 5$) were homogenized in sample buffer (50 mM Tris-HCl pH = 7.6, 10 mM NaCl, 5 mM EDTA, 0.5% Triton-100, 0.1% PIC, 0.1% PHIC 1, 0.1% PHIC 2, 0.1% PHIC 3, PMSF). Laemmli buffer (0.35 M Tris-HCl, 4% SDS, 30% glycerol, 9.3% DTT, pH 6.8, 0.01% bromphenol blue) was added to all samples and boiled at 95°C for 5 min. Hundred μg of protein from each sample was separated by SDS-PAGE (12.5% acrylamide gel) prepared in duplicate. The gel was run at 100 V for 50 min, using a mini-vertical gel electrophoresis (Hofer SE 260; Hofer Inc), hereafter transferred to as nitrocellulose membrane (Nitrocellulose Membrane, 0.2 μm ; Bio-Rad) using a Trans-Blot SD Semi-Dry Transfer Cell (Bio-Rad Laboratories) at 200 mA for 90 min. Nonspecific binding to the membrane was blocked with 5% (w/v) BSA (A2153; SIGMA) in TBS-Tween. Then we proceeded to an overnight incubation, at 4°C with gentle agitation with anti-Akt (9272; cell signalling), anti-phospho-Akt (4058; cell signalling), anti-Erk (9102; cell signalling), anti-phospho-Erk (9101; cell signalling), anti-Bcl-2 (2876; cell signalling) or anti-Bax (2772; cell signalling), all antibodies were diluted from 1:1,000. The following membranes were washed and incubated with fluorescently labeled secondary antibodies: Goat anti-Rabbit IRDye 800cw and IRDye 680LT; LI-COR Biosciences, both

diluted to 1:15,000. The membranes were finally washed and the signal detected using an Odyssey Infrared Imaging System scanner at 800 and 700 nm (LI-COR Biosciences). The intensity values of the detected bands were analysed by background method. P-Erk and P-Akt were normalized for the intensity of its non-phosphorylated signal and the ratio of Bax and Bcl-2 intensity was calculated.

Statistical analysis

Values are presented as mean \pm standard error of mean (SEM). Differences between groups were analysed using two-way ANOVA. When significant differences were detected, the Student–Newman–Keuls test was selected to perform pairwise multiple comparisons. $p < 0.05$ was accepted as significant. Mortality rates were compared with Fisher exact test.

Results

General features

Somatic and cardiac growth of all groups is represented in Table 1. Diabetic animals presented reduced weight gain, and atrophic hearts when compared with euglycemic animals, despite comparable LV + S/BW. Plasma glucose was significantly and similarly elevated in the diabetic groups. Other signs usually associated with diabetic state like polyuria, polydipsia and polyphagia were found in these animals (data not shown).

LV chronic pressure-overload imposed by aortic banding induced hypertrophy as observed by the increased LV + S weight/BW, which was positively correlated with LV- P_{ES} ($r = 0.65$, $p < 0.001$). The association of pressure-overload and diabetes increased lung weight/BW suggesting pulmonary congestion and induced myocardial hypertrophy, altogether indicating a more advanced stage of cardiac dysfunction in the DB group.

Table 1 General features of SHAM, BA, DM and DB groups

Parameter	SHAM ($n = 10$)	DM ($n = 10$)	BA ($n = 10$)	DB ($n = 12$)	
BW (g)	393 \pm 15	250 \pm 7*	415 \pm 13 [†]	284 \pm 10* [‡]	D
GW/TL (mg/mm)	56.6 \pm 1.9	34.6 \pm 1.2*	59.9 \pm 1.4 [†]	40.9 \pm 2.1* [‡]	D
LV + SW (g)	1.04 \pm 0.02	0.72 \pm 0.01	1.26 \pm 0.07	1.01 \pm 0.05	PO
LV + S/BW (g/kg)	1.79 \pm 0.05	1.92 \pm 0.06	2.18 \pm 0.09* [†]	2.44 \pm 0.08* [‡]	PO
Lungs/BW (g/kg)	3.80 \pm 0.14	4.7 \pm 0.15*	3.95 \pm 0.10 [†]	5.23 \pm 0.21* [‡]	D, INT
Plasma glucose (mg/dl)	177 \pm 14	443 \pm 7*	175 \pm 18 [†]	427 \pm 13* [‡]	D

BW body weight, GW/TL gastrocnemius muscle weight/tibial length, LV + SW left ventricle plus septum weight

Data are mean \pm SEM. $p < 0.05$: *versus SHAM, [†]versus DM and [‡]versus BA. For the two-way ANOVA: $p < 0.05$ —the result are significant altered by: D diabetes, PO pressure-overload, INT interaction

Mortality rate was null in SHAM and BA, 29% in DM ($n = 4$) and 14% in DB ($n = 2$).

Quantitative histomorphometry and extracellular matrix analysis

At the end of the protocol, cardiomyocyte diameter was significantly higher in DM, BA and DB than in the SHAM group (SHAM $18.2 \pm 0.3 \mu\text{m}$, DM $21.4 \pm 0.4 \mu\text{m}$, BA $22.0 \pm 0.4 \mu\text{m}$, DB $20.6 \pm 0.4 \mu\text{m}$). Both chronic pressure-overload and diabetes mellitus significantly increased cardiomyocyte diameter, while the concomitant presence of the two conditions (DB) did not further enlarged this parameter as confirmed by the significant interaction ($p < 0.001$).

With regard to the ECM, BA animals presented with higher interstitial myocardial fibrosis than SHAM. Diabetes promoted AGE vascular deposition and induced even more fibrosis, together with a slight increase of TGF- β_1 expression, an effect that was similar in DM and DB groups (Table 2). Interestingly, fibrosis significantly correlated with AGE deposition ($r = 0.55$, $p = 0.02$) and both AGE and fibrosis were positively correlated with lung weight/BW (Fibrosis: $r = 0.52$, $p = 0.03$; AGE: $r = 0.50$, $p = 0.004$) and negatively correlated with BW (Fibrosis: $r = -0.56$, $p = 0.01$; AGE: $r = -0.53$, $p = 0.002$).

We chose to evaluate some of the most relevant MMP contributing to myocardial remodelling [39]. ECM changes were evaluated in terms of collagenases (MMP-1), gelatinase-A (MMP-2) and gelatinase-B (MMP-9) activities.

BA group displayed higher pro-MMP-2 and MMP-9 activity than SHAM group. In contrast, DM group showed higher TIMP-1 concentrations and lower MMP-9/TIMP-1 and MMP-1/TIMP-1 ratios, while DB exhibited reduced MMP-1 activity when compared with SHAM animals (Table 2).

Force measurements in isolated cardiomyocytes

Chronic pressure-overload significantly increased maximal F_{active} independently of concomitant presence of diabetes (Fig. 1a). Despite the trend towards higher F_{passive} in diabetic groups, these values were similar between groups when measured at various sarcomere lengths ranging from 1.6 to 2.2 μm (passive length-tension relations, data not shown) and even after setting sarcomere length at 2.2 μm (Fig. 1b). Myofilament Ca^{2+} -sensitivity was significantly increased in BA, DM and DB groups when compared with SHAM (Fig. 1c). The K_{tr} was significantly decreased in all the intervention groups (Fig. 1d). Interestingly, as observed in Fig. 1 e, f, F_{active} correlated positively with LV- P_{ES} ($r = 0.51$, $p = 0.03$) and LV + S/BW ($r = 0.47$, $p = 0.04$).

Molecular changes

Left ventricular expression of MHC- α was significantly decreased in diabetic hearts (DM $0.46 \pm 0.17 \text{ AU}$, $p = 0.003$ and DB $0.34 \pm 0.16 \text{ AU}$, $p = 0.003$ vs. SHAM $1.00 \pm 0.21 \text{ AU}$ and BA $0.95 \pm 0.16 \text{ AU}$). Contrarily, MHC- β was increased in BA group (BA $4.73 \pm 1.19 \text{ AU}$

Table 2 Extracellular matrix changes: fibrosis, advanced glycation end-product deposition (AGE), metalloproteinase (MMP) activity and tissue-specific matrix metalloproteinase inhibitor assessment (TIMP) in SHAM, BA, DM and DB LV samples

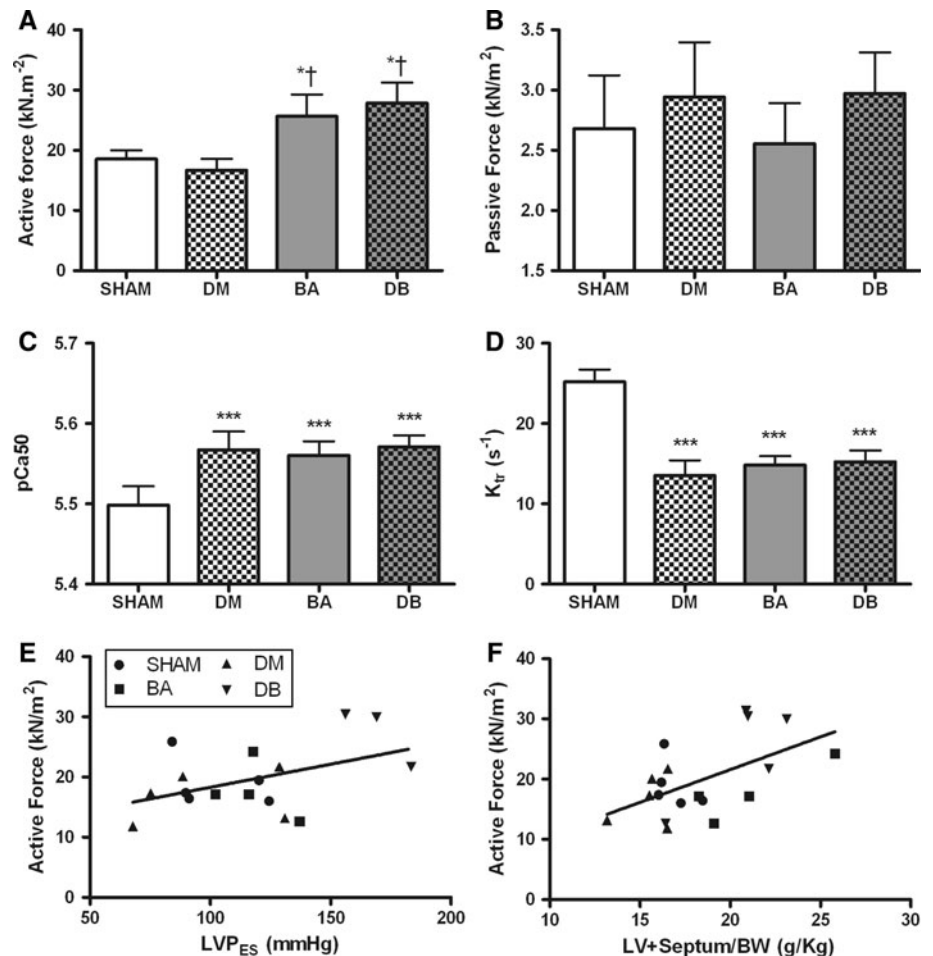
	SHAM	DM	BA	DB	
Interstitial fibrosis (%)	5.3 ± 0.6	$13.9 \pm 1.8^*$	$10.8 \pm 0.9^{*\dagger}$	$13.8 \pm 0.8^{*\ddagger}$	D, PO, INT
AGE (score/ mm^2)	2.1 ± 0.3	$4.9 \pm 0.6^*$	$2.0 \pm 0.4^\dagger$	$5.1 \pm 0.4^{*\ddagger}$	D
TGF- β_1 /GAPDH mRNA (AU)	1.0 ± 0.2	1.5 ± 0.4	0.9 ± 0.2	1.6 ± 0.6	
MMP-1	0.79 ± 0.26	0.74 ± 0.24	0.60 ± 0.17	$0.53 \pm 0.23^*$	INT
Pro-MMP-2 (OD $\text{mm}^2/\text{mg ml protein}$)	0.11 ± 0.04	0.11 ± 0.02	$0.20 \pm 0.01^{*\dagger}$	$0.08 \pm 0.01^\ddagger$	
MMP-2 (OD $\text{mm}^2/\text{mg ml protein}$)	0.69 ± 0.17	0.64 ± 0.21	0.65 ± 0.08	0.67 ± 0.23	
MMP-9 (OD $\text{mm}^2/\text{mg ml protein}$)	0.08 ± 0.02	0.08 ± 0.03	$0.17 \pm 0.03^{*\dagger}$	$0.10 \pm 0.03^\ddagger$	
MMP-1/TIMP-1 (OD $\text{mm}^2/\text{ng/ml}$)	1.60 ± 0.20	$0.54 \pm 0.22^*$	$1.05 \pm 0.31^\dagger$	0.79 ± 0.32	D
MMP-9/TIMP-1 (OD $\text{mm}^2/\text{ng/ml}$)	0.18 ± 0.02	$0.07 \pm 0.02^*$	$0.24 \pm 0.05^\dagger$	0.14 ± 0.05	D
TIMP-1 (ng/ml mg protein)	0.50 ± 0.15	$1.10 \pm 0.53^*$	0.44 ± 0.18	0.46 ± 0.28	
TIMP-2 (ng/ml mg protein)	5.99 ± 0.88	7.05 ± 1.64	6.48 ± 0.78	7.18 ± 2.56	

AGE advanced glycation end-products, TGF- β_1 transforming growth factor- β_1 , MMP-1 collagenase, MMP-2 gelatinase-A, MMP-9 gelatinase-B, TIMP tissue-specific MMP inhibitors

Units of MMPs: OD $\text{mm}^2/\text{mg ml protein}$. Data are mean \pm SEM

$p < 0.05$: *versus SHAM, † versus DM and ‡ versus BA. For the two-way ANOVA: $p < 0.05$ —the results are significantly altered by D diabetes, PO pressure-overload, INT interaction

Fig. 1 Force measurements in single-skinned cardiomyocytes. Maximal active (kN/m^2 , **a**) and passive force (kN/m^2 , **b**), myofilament Ca^{2+} sensitivity (pCa_{50} , **c**), rate constant of force redevelopment (K_{tr} , s^{-1} , **d**), correlation between LV end-systolic pressure and active force ($r = 0.51$, $p = 0.03$, **e**) and correlation between LV + Septum/BW and active force ($r = 0.47$, $p = 0.04$, **f**) in SHAM ($n = 5$), diabetic (DM, $n = 5$), banded (BA, $n = 5$) and diabetic-banded (DB, $n = 5$) animals. Data are mean \pm SEM. $p < 0.05$: *versus SHAM, †versus DM and ‡versus BA



vs. SHAM 1.00 ± 0.15 AU) and further more in the diabetic groups (DM 7.04 ± 1.15 AU, $p = 0.002$ and DB 9.26 ± 1.16 AU, $p = 0.002$). The ratio $\text{MHC-}\alpha/\text{MHC-}\beta$ was, therefore, significantly decreased in overloaded hearts and even more in diabetic conditions (Fig. 2a). Regarding calcium homeostasis, the ratio $\text{SERCA2a}/\text{PLB}$ was similar among groups (Fig. 2b). The myofilament protein phosphorylation status of the different groups was analysed in order to explain some of the observed functional differences (Fig. 2c, d, e). Pressure-overload significantly increased myosin-binding protein C (MyBP-C) phosphorylation and myosin-light-chain-2 phosphorylation (MLC-2), while no significant differences were observed in the phosphorylation status of other myofilament proteins such as Troponin I (TnI, SHAM 1.88 ± 0.31 , DM 1.25 ± 0.25 , BA 1.98 ± 0.29 , DB 1.90 ± 0.34), Troponin T (TnT, SHAM 2.30 ± 0.48 , DM 1.99 ± 0.34 , BA 2.41 ± 0.28 , DB 3.50 ± 0.85), or desmin (SHAM 0.74 ± 0.05 , DM 0.77 ± 0.18 , BA 0.78 ± 0.10 , DB 1.21 ± 0.16). Myocardial inflammation was accessed by measuring $\text{TNF-}\alpha$ expression. We found that diabetes upregulates this pro-inflammatory cytokine (SHAM 1.00 ± 0.18 , DM 1.47 ± 0.30 , BA 0.96 ± 0.19 , DB 1.98 ± 0.58 , $p = 0.04$

for the effect of diabetes). Furthermore, higher $\text{Bax}/\text{Bcl-2}$ ratio was observed, indicating augmented apoptosis in diabetes (Fig. 3a, b, $p = 0.04$).

Concerning insulin-signal pathways, chronic pressure overload increased the ratios of $\text{P-Erk}/\text{Total-Erk}$ ($p = 0.02$) and $\text{P-Akt}/\text{Total-Akt}$ ($p = 0.04$), while the hypoinsulinemia typically associated with the STZ-model significantly decreased $\text{P-Akt}/\text{Total-Akt}$ (Fig. 3c, d, e, f, $p = 0.04$).

In vivo pressure–volume loops analysis

Heart rate was within the published values and presented significantly lower values in the diabetic animals (DM 327 ± 10 bpm, DB 356 ± 11 bpm vs. SHAM 386 ± 9 bpm and BA 388 ± 13 bpm, respectively, $p < 0.001$).

Aortic banding resulted in a significant increase in afterload as observed by the augmented $\text{LV-}P_{ES}$, $\text{LV-}W_{STRESS}$ and arterial elastance (E_a , Fig. 4c) for both BA and DB when compared with SHAM and DM, respectively. Afterload independent assessment of contractility by the ESPVR was significantly lower in both diabetic groups (Fig. 4d).

Fig. 2 Ratio between LV expression of myosin heavy chain- α (MHC)- α /MHC- β (a) and sarcoplasmic reticulum Ca²⁺-ATPase-2a/phospholamban (SERCA2a/PLB, b). Phosphorylation status of myosin-binding-protein-C (pMyBP-C, c) and myosin-light-chain-2 (pMLC-2, d), normalized to total amount of MyBP-C or MLC-2, respectively. Data are mean \pm SEM. $p < 0.05$: *versus SHAM, †versus DM and ‡versus BA. Representative Pro-Q Diamond-stained gels (e) of SHAM ($n = 5$), diabetic (DM, $n = 5$), banded (BA, $n = 5$) and diabetic-banded (DB, $n = 5$) groups

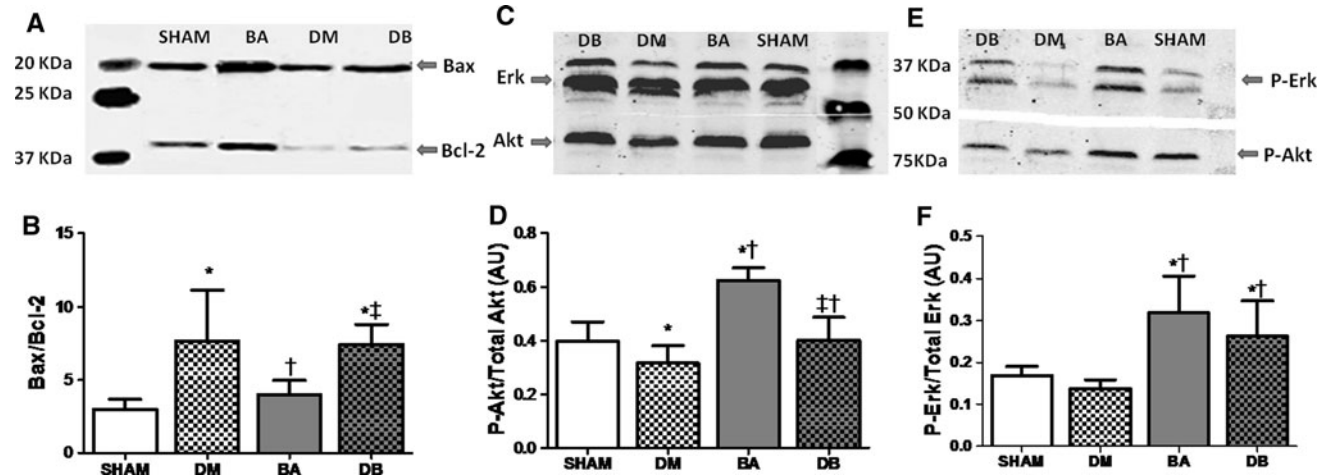
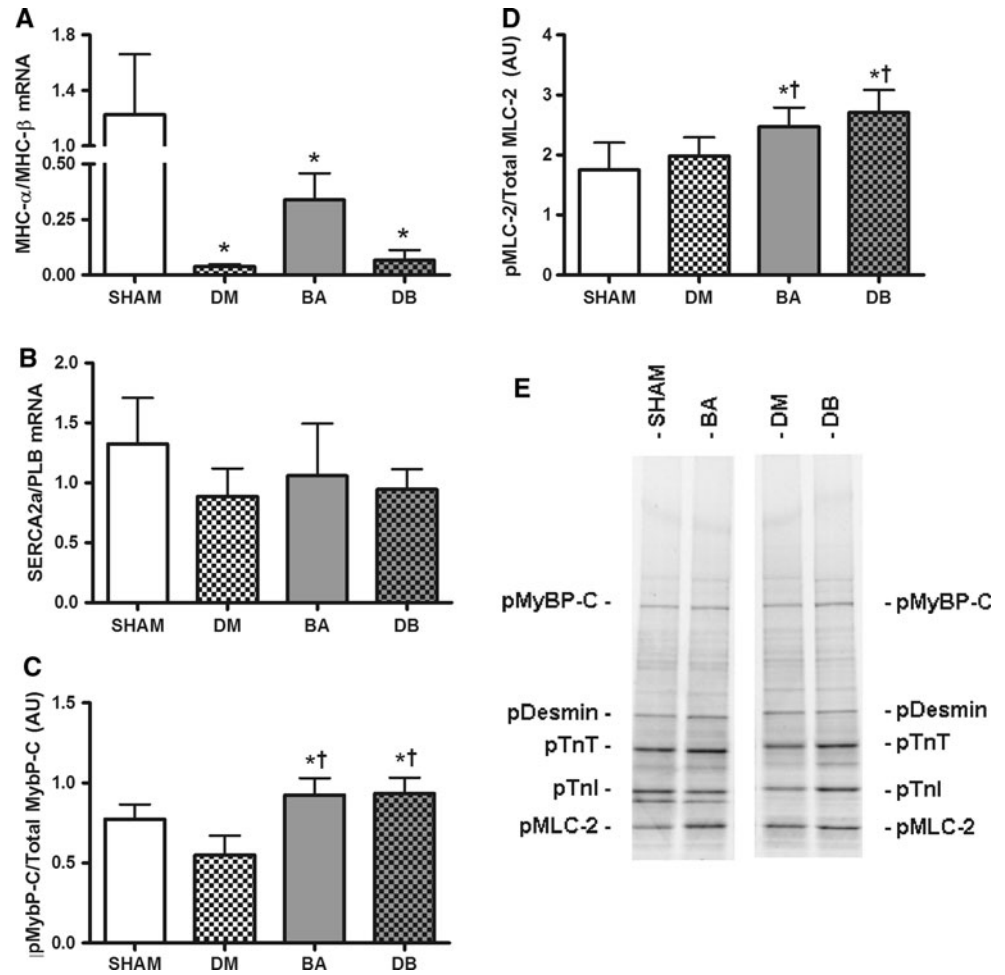
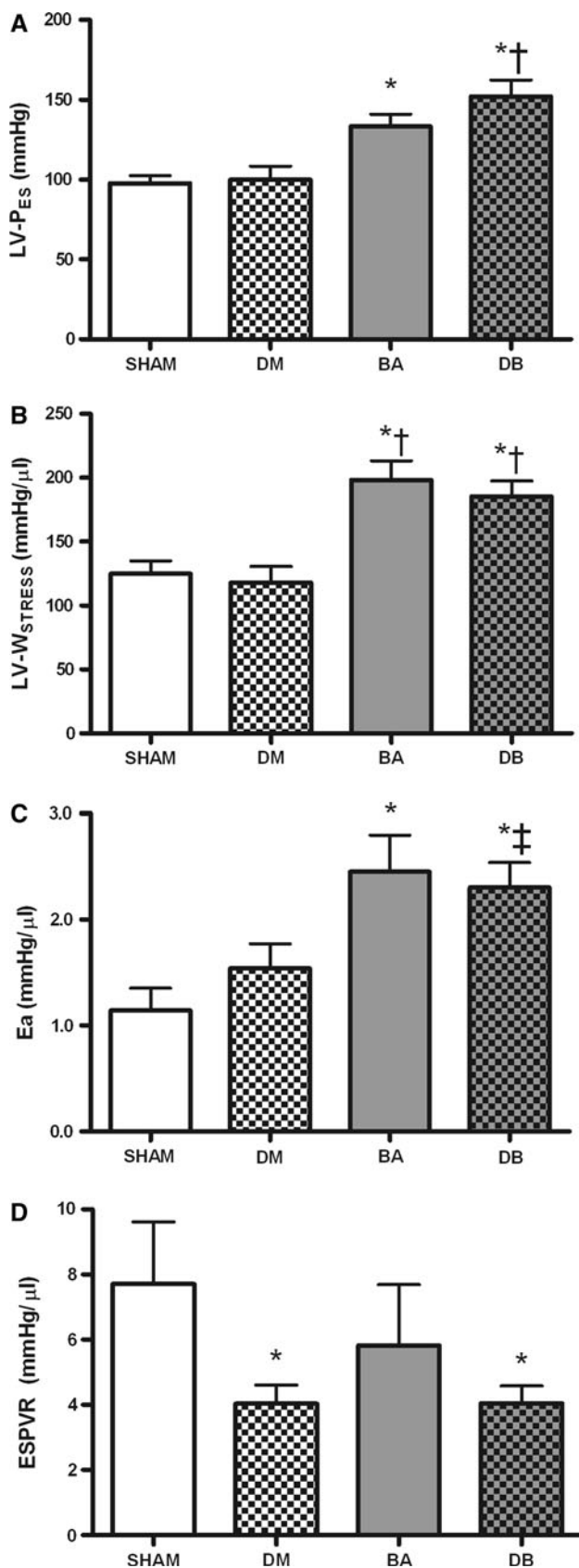


Fig. 3 Western blot analyses of Bax/Bcl-2 ratio (a) revealed that diabetes increases apoptosis in both diabetic groups (DM and DB, $p = 0.04$, b). Pressure overload increased the ratio of phosphorylated/

total Erk (P-Erk/Total-Erk, $p = 0.02$, c, d) and P-Akt/Total-Akt ($p = 0.04$, e, f) while diabetes decreases the latter ($p = 0.04$, e, f). Data are mean \pm SEM. $p < 0.05$: *versus SHAM, †versus DM and ‡versus BA

With regard to diastolic function, relaxation rate, assessed by τ , was significantly prolonged in BA and DB when compared with the non-overloaded animals,

independently of the association with diabetes (Fig. 5a). On the other hand, LV- P_{ED} and EDPVR were significantly increased in the diabetic animals (Fig. 5b, c), indicating



◀ **Fig. 4** In vivo haemodynamic measurements of systolic function. LV end-systolic pressure (LV- P_{ES} , mmHg, **a**); maximal LV wall stress (LV- W_{STRESS} , mmHg/ μ l, **b**); arterial elastance (E_a , mmHg/ μ l, **c**) and end-systolic pressure–volume relation (ESPVR, mmHg/ μ l, **d**) in SHAM ($n = 10$), diabetic (DM, $n = 10$), banded (BA, $n = 10$) and diabetic-banded (DB, $n = 12$) animals. Data are mean \pm SEM. $p < 0.05$: *versus SHAM, †versus DM and ‡versus BA

higher LV stiffness than in euglycemic animals. Interestingly, the higher stiffness of the diabetic myocardium, which was not evident at the myofilament level, became significant in the in vivo haemodynamic setting (representative examples in Fig. 6). Noteworthy E_a was positively correlated with LV- P_{ES} ($r = 0.75$, $p < 0.001$) and that both correlated with hypertrophy (LV + S/BW, $r = 0.51$, $p < 0.01$ and $r = 0.69$, $p < 0.001$, respectively). The relaxation time constant τ correlated with LV hypertrophy (LV + S/BW; $r = 0.32$, $p = 0.03$) while EDPVR correlated with fibrosis ($r = 0.69$, $p = 0.03$) and AGE deposition ($r = 0.41$, $p = 0.04$).

Discussion

Cardiac remodelling is a major determinant of heart failure progression, independently of its aetiology. We found that pressure-overload and diabetes mellitus result in distinct myocardial structural changes leading predominantly to relaxation abnormalities in the first and increased stiffness in the latter.

The main findings reveal that banded animals presented hypertrophied cardiomyocytes whose myofilaments showed augmented F_{active} , MyBP-C and MLC-2 phosphorylation as well as an augmented insulin-signalling activation. At the ECM level, the increased collagen deposition was partially counterbalanced by enhanced gelatinase (pro-MMP-2 and MMP-9) activity. In vivo, myocardial hypertrophy was associated with relaxation abnormalities, as observed by increased τ . Diabetes promoted hypertrophy and decreased K_{tr} . Diabetes-induced drop in K_{tr} is likely to be related with MHC isoform shift. Contrary to banded-animals, insulin-signal pathways were less active as expected by the lower insulin levels. Besides AGE deposition, increased TIMP-1 concentration might have contributed to the observed increase of fibrosis, resulting in stiffer hearts (higher LVP_{ED} and EDPVR). Indeed, lower MMP-9/TIMP-1 and MMP-1/TIMP-1 ratios were observed. These animals presented significant inflammatory activation and increased myocardial apoptosis. The association of diabetes and pressure-overload induced further hypertrophy, prolonged relaxation and increased myocardial stiffness, therefore resulting in more

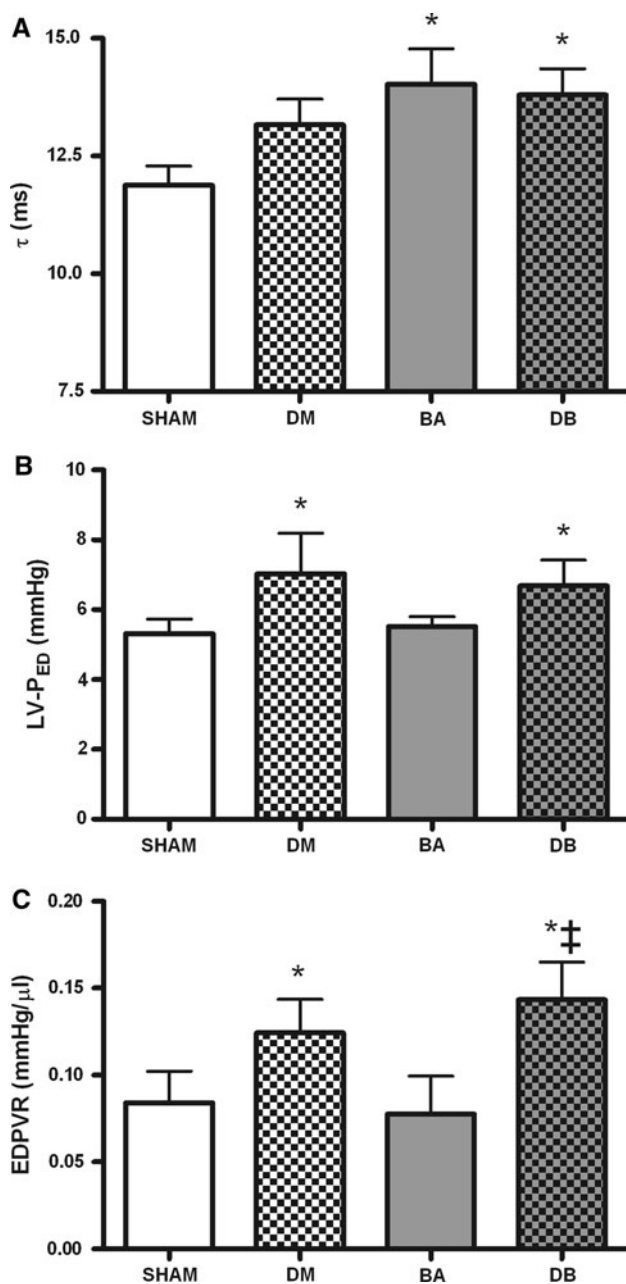


Fig. 5 In vivo haemodynamic measurements of diastolic function. Time constant τ (ms, **a**), end-diastolic pressure (LV- P_{ED} , mmHg, **b**) and end-diastolic pressure–volume relation (EDPVR, mmHg/ μ l, **c**) in SHAM ($n = 10$), diabetic (DM, $n = 10$), banded (BA, $n = 10$) and diabetic-banded (DB, $n = 12$) animals. Data are mean \pm SEM. $p < 0.05$: *versus SHAM, [†]versus DM and [‡]versus BA

severe diastolic dysfunction and worse pulmonary congestion in DB animals.

Effects of chronic pressure-overload

Chronic pressure-overload can be experimentally induced by supra-renal aortic constriction. This model displays low

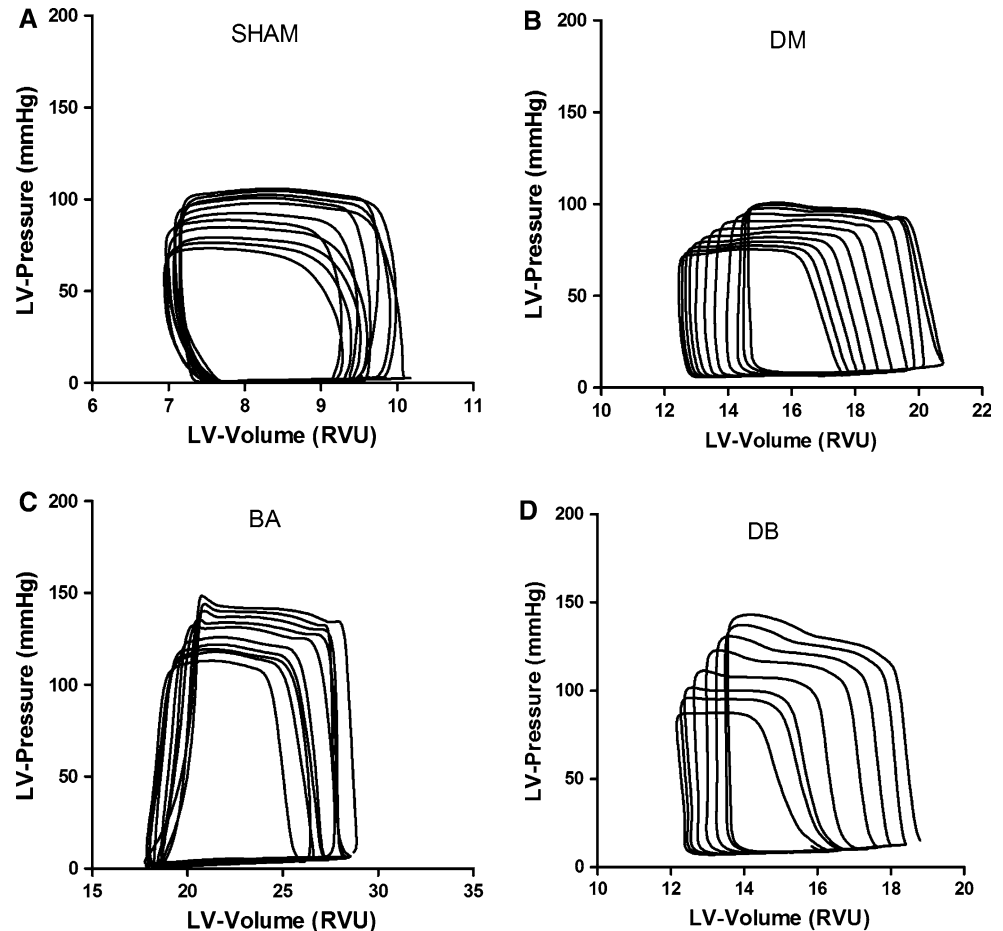
mortality rate, activation of hypertrophy-inducing neuro-humoral systems, such as the renin-angiotensin-aldosterone-system (RAAS), and substantial LV mass increase when compared with similar models such as transverse aortic constriction [49].

As expected, chronic pressure-overload increased LV- P_{ES} , arterial elastance and LV- W_{STRESS} with concomitant hypertrophy. Persistent elevation of LV- P_{ES} even after hypertrophy indicates that the hypertrophic response was not enough to normalize afterload at this stage. Interestingly, pressure-overload significantly increased myofilaments' F_{active} and Ca^{2+} sensitivity indicating that the higher LV- P_{ES} is not only a consequence of cardiomyocytes' enlargement, but also of changes in myofilaments intrinsic properties. The positive correlation between F_{active} , LV + S/BW and LV- P_{ES} , highlights the integration of this hypertrophy-induced remodelling at different levels of myocardial organization: from cardiomyocytes myofilaments to the whole heart.

Postranslational modification of contractile proteins represents a very relevant area within myofilament protein research. It is well known that phosphorylation status of myofilament proteins modulates contractility and relaxation. Currently, MyBP-C is implicated in the kinetics of crossbridge cycling and modulation of force production [47]. However, the exact physiological function of its phosphorylation in healthy or in HF myocardium remains unclear. In the present study, we found increased MyBP-C phosphorylation in the presence of pressure-overload-induced hypertrophy consistent with the increased myofilament F_{active} . Hyperphosphorylation of MyBP-C may result from an increase of PKA-induced β -adrenergic stimulation during hypertrophy progression [12]. Accordingly, transgenic mice lacking the MyBP-C phosphorylation sites displayed depressed cardiac contractility [35]. In addition, several studies suggest a direct relationship between the percentage of phosphorylated MyBP-C and cardiomyocytes' maximal force [26]. MLC-2 was also found to be increased in the overloaded groups. Upon phosphorylation, this regulatory protein is able to modulate myosin–actin interaction via actin-activated ATPase activity, increasing the force developed by the myofilaments at submaximal Ca^{2+} concentration, which indicates an augmented Ca^{2+} sensitivity as herein demonstrated [40]. Increased MLC-2 phosphorylation has been described in hypertrophied hearts as a compensatory response to enhance contractile performance and efficiency [19]. These results are in agreement with the increased contractility and myofilament F_{active} that we found in BA and DB animals and further support our integrative hypertrophic response.

Regarding diastolic abnormalities, prolonged relaxation observed in banded animals was positively correlated with increased LV- P_{ES} and hypertrophy, consistent with

Fig. 6 **a** Representative pressure–volume loops from each experimental group during vena cava occlusion, showing increased LV end-systolic pressure in both banded groups while diabetic animals presented increased stiffness (LV- P_{ED}). **a** SHAM; **b** diabetic (DM); **c** banded (BA) and **d** diabetic-banded (DB) rats



previous studies indicating that severe or late-systolic loading is accompanied by premature LV pressure fall and slower relaxation [23]. Furthermore, pressure-overload induced an increase in pro-MMP-2 and MMP-9, without being counterbalanced by an increase of TIMP tissue concentration. In fact, in a compensated stage of hypertrophy, this increase results from alterations in the myocardial environment in response to the hypertrophic stimulus, such as mechanical stress, neurohumoral activation and release of inflammatory mediators [42]. Particularly, transgenic mice lacking MMP-9 and MMP-2 have shown the ability to prevent cardiac rupture, and decreased cardiac dilatation and dysfunction after acute myocardial infarction [15, 18], revealing the important role of gelatinases in the remodeling process associated with cardiac hypertrophy.

The insulin-signal transduction pathway regulates several aspects of cellular physiology, including most notably the regulation of cellular growth and of glucose uptake and utilization [8]. When insulin binds to insulin receptor it activates a complex signal transduction network. The phosphatidylinositol 3-kinase (PI3K) acting via Akt/PKB and the MAPK/ERK are the two main pathways of that network. PI3K is considered the main player of the

metabolic action of insulin, whereas the MAPK/Erk pathway is mainly involved in cell growth and differentiation. Akt phosphorylates a variety of intracellular substrates such as glycogen synthase kinase-3 (GSK-3) and the forkhead box O (FOXO) transcription factor family, regulating cell growth, metabolism and glucose uptake. We found that chronic pressure overload was able to increase insulin signalling both via Erk and via Akt pathways, therefore supporting the idea that insulin is an important regulator of physiological cardiac growth and muscle metabolism. In line with our studies, previous studies demonstrated that some pathological conditions, such as hypertension, are linked to the chronic stimulation of PI3K/PKB/Akt and/or MAPK pathways, which undeniably participate in the establishment of myocardial hypertrophy [3].

Effects of diabetes mellitus

In addition to fibrosis, which has been extensively associated with diabetes [44], other post-translational modifications can alter ECM. Irreversibly formed biochemical end products of non-enzymatic glycation, AGE, compromise myocardial stiffness and interact with RAGE inducing

further fibrosis and activating a pro-inflammatory programme. In fact, we demonstrated that vascular deposition of AGE correlated positively with fibrosis and stiffness and was substantially increased in DM and DB which is consistent with previous reports that demonstrated that plasma [3], arterial wall [6] and myocardial levels [2] of AGE correlate positively with ventricular filling impairment, indicating a role for AGE in myocardial stiffening of type-I diabetic heart patients [3].

Regarding myofilament changes, diabetes induced a significant drop in K_{tr} , which is likely to be related with MHC isoform shift. One of the major isoform changes is the shift from the fast MHC- α to the slow and more economical MHC- β , representing an attempt to compensate for the metabolic changes that take place in the diabetic heart [14] and contributing to decreased contractility such as the reduced ESPVR herein described.

In DM and DB animals, decreased MMP activity, particularly MMP-9/TIMP-1 and MMP-1/TIMP-1, may have prevented collagen degradation, enhanced its deposition and presumably contributed to increase myocardial stiffness in diabetic cardiomyopathy. Indeed, Li et al. [24] had previously shown that total collagen content correlated negatively with the activity and expression of MMP-2 and correlated positively with TIMP-1 expression in the myocardium of diabetic rats.

Also a similar situation was shown in the most advanced stages of other heart diseases associated with cardiac dysfunction [29]. In the present study, MMP-2 activity was, however, similar amongst all groups, which diverges from a previous study where reduced MMP-2 activity was responsible for the ECM changes observed STZ-rats with the same duration of diabetes [45]. It is currently accepted that MMP-2 activity is inhibited by TIMP-2 and its expression increased by TGF- β 1 signalling, via Smad 7 [45] and Smad 2/3 activation [36]. In our study we found a tendency for both TIMP-2 and TGF- β 1 to increase. Although not significant, this slight increase may reconcile the differences herein reported. Moreover, several animal models have demonstrated a time-dependent change in MMP expression and activity according to the extent of myocardial remodelling [38]: increasing in compensated hypertrophy, but decreasing throughout progression to HF [27], even when ejection fraction was still preserved [29, 42].

We should emphasize that sometimes semi-quantitative assessment of cardiac fibrosis may not allow dissecting the effects of pressure-overload from those associated with diabetes. In our experiment different patterns of MMP activities and TIMP concentrations were observed in the two conditions, inasmuch as the fibrosis observed in banded rats was associated with increased MMP activity, enhancing enzymatic collagen degradation, whereas diabetes-related ECM deposition was coupled with increased TIMP

concentration, i.e. higher inhibition of collagenolytic activity. These data indicate that cardiac fibrosis progression during either chronic pressure-overload or experimental diabetes induces different mechanisms in the ECM turnover process. In the former condition, increased afterload stimulates collagen deposition and enhanced MMP lytic activity, whereas in the latter metabolic changes are associated with increased TIMP concentrations, which inhibit ECM degradation, promoting further fibrosis. The present experiment indicates that these qualitative differences in collagen deposition are associated with a different pattern of ECM turnover, as it can be gauged from the assessment of myocardial MMP activity and TIMP concentration.

Last, diabetic, but not the overloaded animals presented signs of myocardial inflammation as indicated by the observed upregulation of TNF- α , which is in line with previous finding [22]. Volz et al. showed that sustained pro-inflammatory signalling in the adult heart from transgenic mice overexpressing myocardial TNF- α is associated with a pro-fibrotic phenotype that arises, at least in part, from TGF- β 1-mediated signalling, leading to increased myocardial fibrosis and increased LV diastolic chamber stiffness. Indeed, recently, high mobility group box 1 (HMGB1) has been identified as a potent innate “danger signal” for the initiation of host defence or tissue repair. By interacting with RAGE and activating NF- κ B, this factor mediates pro-inflammatory effects [46]. It was also described that sustained activation of NF- κ B under marked hyperglycaemic conditions regulates the expression of effectors such as TNF- α , IL-6 and TGF- β 1. Although we did not specifically evaluate HMGB1 levels we have reasonable evidence (increased expression of TNF- α and TGF- β 1) to suggest that this pathway is probably involved in myocardial injury observed in the diabetic groups.

Regarding insulin-signal transduction pathway, we found that diabetes decreased Akt/PKB signalling, which is consonant with the hypoinsulinaemic environment that characterizes STZ-rats. STZ-induced diabetes has been associated with myocardial atrophy [30], associated with loss of contractile proteins, myocyte apoptosis and increased interstitial fibrosis, as herein reported, and consistent with the absence of the mitogenic and prosurvival effects of insulin [30].

Effects of concomitant chronic pressure-overload and diabetes mellitus

Concomitant pressure overload and diabetes gather relaxation abnormalities and stiffer hearts. Altogether, this resulted in further LV hypertrophy and lung congestion, decreased phosphorylation of Akt, leading to a worse general diastolic dysfunction condition. Previous studies on

the effects of hypertension and diabetes on intrinsic myocardial function showed that they were additive, with the greatest abnormalities resulting from the combination of these two interventions [11, 34]. Diabetic banded animals, which represent a worse state of decompensate hypertrophy, hold a more severe diastolic dysfunction as they present both overload-induced impaired relaxation and diabetes-induced increased chamber stiffness.

We conclude that diabetes mellitus and chronic pressure overload led to distinct phenotypes: while overloaded animals presented with relaxation abnormalities, the diabetics developed not only impaired relaxation but also, and presumably more importantly, stiffer ventricles. Association of overload and diabetes combines these damages in a way that precipitates a faster progression to diastolic dysfunction and heart failure.

Acknowledgments The authors would like to thank Doctor José Magalhães and his group for kindly providing anti-Bax and anti-Bcl-2 antibodies. This work was supported by the Portuguese Foundation for Science and Technology (grant number PIC/IC/82943/2007) through the Cardiovascular R&D Unit (FCT nr. 51/94) and by the European Union Project FP7-HEALTH-2010: “MEDIA-Metabolic Road to Diastolic Heart Failure”. #HEALTH. 2010.2.4.2-4.

Conflict of interest None.

References

- Anversa P, Li P, Malhotra A, Zhang X, Herman MV, Capasso JM (1993) Effects of hypertension and coronary constriction on cardiac function, morphology, and contractile proteins in rats. *Am J Physiol* 265:H713–H724
- Aronson D (2003) Cross-linking of glycated collagen in the pathogenesis of arterial and myocardial stiffening of aging and diabetes. *J Hypertens* 21:3–12. doi:10.1097/01.hjh.0000042892.24999.92
- Berg TJ, Snorgaard O, Faber J, Torjesen PA, Hildebrandt P, Mehlsen J, Hanssen KF (1999) Serum levels of advanced glycation end products are associated with left ventricular diastolic function in patients with type 1 diabetes. *Diabetes Care* 22:1186–1190. doi:10.2337/diacare.22.7.1186
- Borbely A, van der Velden J, Papp Z, Bronzwaer JG, Edes I, Stienen GJ, Paulus WJ (2005) Cardiomyocyte stiffness in diastolic heart failure. *Circulation* 111:774–781. doi:10.1161/01.CIR.0000155257.33485.6D
- Brown RA, Filipovich P, Walsh MF, Sowers JR (1996) Influence of sex, diabetes and ethanol on intrinsic contractile performance of isolated rat myocardium. *Basic Res Cardiol* 91:353–360. doi:10.1007/BF00788714
- Brownlee M, Cerami A, Vlassara H (1988) Advanced glycosylation end products in tissue and the biochemical basis of diabetic complications. *N Engl J Med* 318:1315–1321. doi:10.1056/NEJM198805193182007
- Capasso JM, Palackal T, Olivetti G, Anversa P (1990) Left ventricular failure induced by long-term hypertension in rats. *Circ Res* 66:1400–1412
- DeBosch BJ, Muslin AJ (2008) Insulin signaling pathways and cardiac growth. *J Mol Cell Cardiol* 44:855–864. doi:10.1016/j.jmcc.2008.03.008
- Dhalla NS, Liu X, Panagia V, Takeda N (1998) Subcellular remodeling and heart dysfunction in chronic diabetes. *Cardiovasc Res* 40:239–247. doi:10.1016/S0008-6363(98)00186-2
- Dubrey SW, Reaveley DR, Seed M, Lane DA, Ireland H, O'Donnell M, O'Connor B, Noble MI, Leslie RD (1994) Risk factors for cardiovascular disease in IDDM. A study of identical twins. *Diabetes* 43:831–835
- Fein FS, Zola BE, Malhotra A, Cho S, Factor SM, Scheuer J, Sonnenblick EH (1990) Hypertensive-diabetic cardiomyopathy in rats. *Am J Physiol* 258:H793–H805. doi:10.2337/diabetes.43.6.831
- Gautel M, Zuffardi O, Freiburg A, Labeit S (1995) Phosphorylation switches specific for the cardiac isoform of myosin binding protein-C: a modulator of cardiac contraction? *EMBO J* 14:1952–1960
- Grossman E, Messerli FH (1996) Diabetic and hypertensive heart disease. *Ann Intern Med* 125:304–310
- Gupta MP (2007) Factors controlling cardiac myosin-isoform shift during hypertrophy and heart failure. *J Mol Cell Cardiol* 43:388–403. doi:10.1016/j.jmcc.2007.07.045
- Hayashidani S, Tsutsui H, Ikeuchi M, Shiomi T, Matsusaka H, Kubota T, Imanaka-Yoshida K, Itoh T, Takeshita A (2003) Targeted deletion of MMP-2 attenuates early LV rupture and late remodeling after experimental myocardial infarction. *Am J Physiol Heart Circ Physiol* 285:H1229–H1235. doi:10.1152/ajpheart.00207.2003
- Hessel MH, Steendijk P, den Adel B, Schutte CI, van der Laarse A (2006) Characterization of right ventricular function after monocrotaline-induced pulmonary hypertension in the intact rat. *Am J Physiol Heart Circ Physiol* 291:H2424–H2430. doi:10.1152/ajpheart.00369.2006
- Heusch G (2009) Diastolic heart failure: a misNomer. *Basic Res Cardiol* 104:465–467. doi:10.1007/s00395-009-0025-3
- Heymans S, Lutun A, Nuyens D, Theilmeier G, Creemers E, Moons L, Dyspersin GD, Cleutjens JP, Shipley M, Angellilo A, Levi M, Nube O, Baker A, Keshet E, Lupu F, Herbert JM, Smits JF, Shapiro SD, Baes M, Borgers M, Collen D, Daemen MJ, Carmeliet P (1999) Inhibition of plasminogen activators or matrix metalloproteinases prevents cardiac rupture but impairs therapeutic angiogenesis and causes cardiac failure. *Nat Med* 5:1135–1142. doi:10.1038/13459
- Huang J, Shelton JM, Richardson JA, Kamm KE, Stull JT (2008) Myosin regulatory light chain phosphorylation attenuates cardiac hypertrophy. *J Biol Chem* 283:19748–19756. doi:10.1074/jbc.M802605200
- Ihm SH, Chang K, Kim HY, Baek SH, Youn HJ, Seung KB, Kim JH (2010) Peroxisome proliferator-activated receptor-gamma activation attenuates cardiac fibrosis in type 2 diabetic rats: the effect of rosiglitazone on myocardial expression of receptor for advanced glycation end products and of connective tissue growth factor. *Basic Res Cardiol* 105:399–407. doi:10.1007/s00395-009-0071-x
- Junqueira LC, Bignolas G, Brentani RR (1979) Picrosirius staining plus polarization microscopy, a specific method for collagen detection in tissue sections. *Histochem J* 11:447–455. doi:10.1007/BF01002772
- Kleinbongard P, Heusch G, Schulz R (2010) TNFalpha in atherosclerosis, myocardial ischemia/reperfusion and heart failure. *Pharmacol Ther* 127:295–314. doi:10.1016/j.pharmthera.2010.05.002
- Leite-Moreira AF (2006) Current perspectives in diastolic dysfunction and diastolic heart failure. *Heart* 92:712–718. doi:10.1136/hrt.2005.062950
- Li Q, Sun SZ, Wang Y, Tian YJ, Liu MH (2007) The roles of MMP-2/TIMP-2 in extracellular matrix remodelling in the hearts of STZ-induced diabetic rats. *Acta Cardiol* 62:485–491. doi:10.2143/AC.62.5.2023412

25. Litwin SE, Raya TE, Anderson PG, Daugherty S, Goldman S (1990) Abnormal cardiac function in the streptozotocin-diabetic rat. Changes in active and passive properties of the left ventricle. *J Clin Invest* 86:481–488. doi:[10.1172/JCI114734](https://doi.org/10.1172/JCI114734)
26. McClellan G, Kulikovskaya I, Winegrad S (2001) Changes in cardiac contractility related to calcium-mediated changes in phosphorylation of myosin-binding protein C. *Biophys J* 81:1083–1092. doi:[10.1016/S0006-3495\(01\)75765-7](https://doi.org/10.1016/S0006-3495(01)75765-7)
27. Nagatomo Y, Carabello BA, Coker ML, McDermott PJ, Nemoto S, Hamawaki M, Spinale FG (2000) Differential effects of pressure or volume overload on myocardial MMP levels and inhibitory control. *Am J Physiol Heart Circ Physiol* 278:H151–H161
28. Perlini S, Palladini G, Ferrero I, Tozzi R, Fallarini S, Facchetti A, Nano R, Clari F, Busca G, Fogari R, Ferrari AU (2005) Sympathectomy or doxazosin, but not propranolol, blunt myocardial interstitial fibrosis in pressure-overload hypertrophy. *Hypertension* 46:1213–1218
29. Polyakova V, Hein S, Kostin S, Ziegelhoeffer T, Schaper J (2004) Matrix metalloproteinases and their tissue inhibitors in pressure-overloaded human myocardium during heart failure progression. *J Am Coll Cardiol* 44:1609–1618. doi:[10.1016/j.jacc.2004.07.023](https://doi.org/10.1016/j.jacc.2004.07.023)
30. Poornima IG, Parikh P, Shannon RP (2006) Diabetic cardiomyopathy: the search for a unifying hypothesis. *Circ Res* 98:596–605. doi:[10.1161/01.RES.0000207406.94146.c2](https://doi.org/10.1161/01.RES.0000207406.94146.c2)
31. Regan TJ, Khan MI, Ettinger PO, Haider B, Lyons MM, Oldewurtel HA (1974) Myocardial function and lipid metabolism in the chronic alcoholic animal. *J Clin Invest* 54:740–752. doi:[10.1172/JCI107812](https://doi.org/10.1172/JCI107812)
32. Ren J, Davidoff AJ (1997) Diabetes rapidly induces contractile dysfunctions in isolated ventricular myocytes. *Am J Physiol* 272:H148–H158
33. Riva E, Andreoni G, Bianchi R, Latini R, Luvara G, Jeremic G, Traquandi C, Tuccinardi L (1998) Changes in diastolic function and collagen content in normotensive and hypertensive rats with long-term streptozotocin-induced diabetes. *Pharmacol Res* 37:233–240. doi:[10.1006/phrs.1998.0290](https://doi.org/10.1006/phrs.1998.0290)
34. Rodgers RL, Davidoff AJ, Mariani MJ (1991) Cardiac function of the diabetic renovascular hypertensive rat: effects of insulin and thyroid hormone treatment. *Can J Physiol Pharmacol* 69:346–354. doi:[10.1139/y91-053](https://doi.org/10.1139/y91-053)
35. Sadayappan S, Gulick J, Osinska H, Martin LA, Hahn HS, Dorn GW 2nd, Kleivitsky R, Seidman CE, Seidman JG, Robbins J (2005) Cardiac myosin-binding protein-C phosphorylation and cardiac function. *Circ Res* 97:1156–1163. doi:[10.1161/01.RES.0000190605.79013.4d](https://doi.org/10.1161/01.RES.0000190605.79013.4d)
36. Sakata Y, Chancey AL, Divakaran VG, Sekiguchi K, Sivasubramanian N, Mann DL (2008) Transforming growth factor-beta receptor antagonism attenuates myocardial fibrosis in mice with cardiac-restricted overexpression of tumor necrosis factor. *Basic Res Cardiol* 103:60–68. doi:[10.1007/s00395-007-0689-5](https://doi.org/10.1007/s00395-007-0689-5)
37. Schalkwijk CG, Baidoshvili A, Stehouwer CD, van Hinsbergh VW, Niessen HW (2004) Increased accumulation of the glycoxidation product Nepsilon-(carboxymethyl)lysine in hearts of diabetic patients: generation and characterisation of a monoclonal anti-CML antibody. *Biochim Biophys Acta* 1636:82–89
38. Spinale FG (2002) Matrix metalloproteinases: regulation and dysregulation in the failing heart. *Circ Res* 90:520–530. doi:[10.1016/S0008-6363\(99\)00431-9](https://doi.org/10.1016/S0008-6363(99)00431-9)
39. Spinale FG, Coker ML, Bond BR, Zellner JL (2000) Myocardial matrix degradation and metalloproteinase activation in the failing heart: a potential therapeutic target. *Cardiovasc Res* 46:225–238. doi:[10.1016/S0008-6363\(99\)00431-9](https://doi.org/10.1016/S0008-6363(99)00431-9)
40. Sweeney HL, Bowman BF, Stull JT (1993) Myosin light chain phosphorylation in vertebrate striated muscle: regulation and function. *Am J Physiol* 264:C1085–C1095
41. Tomlinson KC, Gardiner SM, Hebden RA, Bennett T (1992) Functional consequences of streptozotocin-induced diabetes mellitus, with particular reference to the cardiovascular system. *Pharmacol Rev* 44:103–150
42. Tozzi R, Palladini G, Fallarini S, Nano R, Gatti C, Presotto C, Schiavone A, Micheletti R, Ferrari P, Fogari R, Perlini S (2007) Matrix metalloprotease activity is enhanced in the compensated but not in the decompensated phase of pressure overload hypertrophy. *Am J Hypertens* 20:663–669. doi:[10.1016/j.amjhyper.2007.01.016](https://doi.org/10.1016/j.amjhyper.2007.01.016)
43. van Heerebeek L, Borbely A, Niessen HW, Bronzwaer JG, van der Velden J, Stienen GJ, Linke WA, Laarman GJ, Paulus WJ (2006) Myocardial structure and function differ in systolic and diastolic heart failure. *Circulation* 113:1966–1973. doi:[10.1161/CIRCULATIONAHA.105.587519](https://doi.org/10.1161/CIRCULATIONAHA.105.587519)
44. van Hoeven KH, Factor SM (1990) A comparison of the pathological spectrum of hypertensive, diabetic, and hypertensive-diabetic heart disease. *Circulation* 82:848–855
45. Van Linthout S, Seeland U, Riad A, Eckhardt O, Hohl M, Dhayat N, Richter U, Fischer JW, Bohm M, Pauschinger M, Schultheiss HP, Tschope C (2008) Reduced MMP-2 activity contributes to cardiac fibrosis in experimental diabetic cardiomyopathy. *Basic Res Cardiol* 103:319–327. doi:[10.1007/s00395-008-0715-2](https://doi.org/10.1007/s00395-008-0715-2)
46. Volz HC, Seidel C, Laohachewin D, Kaya Z, Muller OJ, Plegier ST, Lasitschka F, Bianchi ME, Remppis A, Bierhaus A, Katus HA, Andrassy M (2010) HMGB1: the missing link between diabetes mellitus and heart failure. *Basic Res Cardiol* 105:805–820. doi:[10.1007/s00395-010-0114-3](https://doi.org/10.1007/s00395-010-0114-3)
47. Weisberg A, Winegrad S (1998) Relation between crossbridge structure and actomyosin ATPase activity in rat heart. *Circ Res* 83:60–72
48. Whittaker P, Kloner RA, Boughner DR, Pickering JG (1994) Quantitative assessment of myocardial collagen with picosirius red staining and circularly polarized light. *Basic Res Cardiol* 89:397–410. doi:[10.1007/BF00788278](https://doi.org/10.1007/BF00788278)
49. Wiesner RJ, Ehmke H, Faulhaber J, Zak R, Ruegg JC (1997) Dissociation of left ventricular hypertrophy, beta-myosin heavy chain gene expression, and myosin isoform switch in rats after ascending aortic stenosis. *Circulation* 95:1253–1259
50. Yang B, Larson DF, Watson R (1999) Age-related left ventricular function in the mouse: analysis based on in vivo pressure-volume relationships. *Am J Physiol* 277:H1906–H1913
51. Zaremba R, Merkus D, Hamdani N, Lamers JML, Paulus WJ, dos Remedios C, Duncker DJ, Stienen GJM, van der Velden J (2007) Quantitative analysis of myofilament protein phosphorylation in small cardiac biopsies. *Proteomics Clin Appl* 1:1285. doi:[10.1002/prca.200600891](https://doi.org/10.1002/prca.200600891)
52. Zile MR, Baicu CF, Gaasch WH (2004) Diastolic heart failure—abnormalities in active relaxation and passive stiffness of the left ventricle. *N Engl J Med* 350:1953–1959. doi:[10.1056/NEJMoa032566](https://doi.org/10.1056/NEJMoa032566)